

Processing Optimization and Characterization of Magnetic Non-Oriented Electrical Silicon Steel

R. Ramadan¹, S.A Ibrahim^{1,*}, M. Farag², A.A. Elzatahry³, M. H. Es-Saheb⁴

¹ Faculty of Petroleum & Mining Engineering, Suez Canal University, Egypt

² Kandil Steel Complex, 10th of Ramadan City, Egypt

³ Petrochemical research chair, Department of Chemistry, King Saud University, Riyadh, Kingdom of Saudi Arabia.

⁴ Mechanical Engineering Dept., King Saud University, Riyadh, Kingdom of Saudi Arabia.

*E-mail: samirabdalhakim@yahoo.com

Received: 6 January 2012 / Accepted: 3 March 2012 / Published: 1 April 2012

In this study, the improvement of magnetic properties of non-oriented electrical sheet steel has been achieved through the optimization of various processing parameters. The optimized grain size after decarburizing annealing is related to the lowest watt loss and highest magnetic permeability values. The percentage of cold rolling is examined with primary recrystallization annealing regimes that are proposed followed with different percentages of temper rolling and final two different decarburizing annealing regimes and their impact on magnetic properties results are evaluated. Micro structures, magnetic properties mechanical properties are measured and evaluated in relation to EN standard of electrical steel. The hysteresis curves for the final decarburized samples related to various temper rolling reduction is plotted and evaluated.

Keywords: Non-oriented electrical steel, watt loss, magnetic permeability, Cold rolling, primary recrystallization annealing, temper rolling, decarburizing annealing treatment.

1. INTRODUCTION

Non-oriented electrical steel sheets are widely used in various electrical industries applications such as small motors, transformers and electrical rotating machine [1,2]. Few studies on different properties of non oriented electrical steel sheets have been published [3-7]. Many factors including process variables for the electrical sheet steel production have been found to have a greater influence on the overall magnetic properties [8-14]. However, there is no single parameter which can comprehensively describe the magnetic behavior of the material due to the complex interaction of

large variables which affect magnetic properties of steel especially watt loss and magnetic permeability. Therefore, optimization of the process parameters such as the amount of cold rolling reduction, primary recrystallization annealing regime, temper rolling reduction and decarburization annealing conditions are essential to compromise the lowest watt loss and highest permeability values. In the present work, various amount of cold rolling reduction and its effects on recrystallization processes are examined. Also, various temper rolling reductions are suggested with two different decarburization annealing regimes for the primary recrystallization annealed material.

2. EXPERIMENTAL PROCEDURES

2.1 Material Processing

Hot rolled electrical silicon steel coils supplied by ANSDK Company (Alexandria, Egypt) with chemical composition given in Table (1) are used in this investigation. The hot rolled samples are supplied with commercial hot band thickness 2.0 ± 0.02 mm.

Table 1. Chemical composition of the hot rolled steel.

C. wt%	Mn.wt%	S.wt%	P.wt%	Si.wt%	N.wt%	Al.wt%	Material type
0.045	0.236	0.0010	0.067	0.62	50ppm	0.289	Al-killed steel

Hot rolled coils were pickled prior to cold rolling by using Hydraulic acid (HCL) at 80°C to remove the heavy adhesive surface oxides due to presence of silicon in that steel, then cold rolled with various reductions of 65,70 and 75% in four high reverse cold rolling mills. Annealing is carried out in bell furnaces (Batch-type) using a mixture of 25% N_2 and 75% H_2 in order to protect the surface.

The samples are heated to annealing temperature 740°C through heating rate of $62^{\circ}\text{C}/\text{hr.}$, then soaked for 20 hrs., finally decreasing the annealing temperature to 650°C over a period of 4 hrs. Cooling is done in three steps to 500°C and then to 350°C under cooling bell up to exit temperature of 80°C are used.

Temper rolling process is carried out using four high reverse mill with applying different temper rolling reductions of 3, 5, 7 and 9% using smooth work roll with $1.5 \mu\text{m}$ surface roughness and typical temper conditions.

Grain growth decarburization annealing was conducted using two different conditions. The first condition is carried out in decarburizing continuous annealing furnaces with protective atmosphere $\text{CO}_2, \text{CO}, \text{H}_2, \text{N}_2$ with CO_2/CO ratio > 0.5 atmosphere, at $770-790^{\circ}\text{C}$ for 5.2 hrs., annealing. Meanwhile, the second process decarburizing annealing is carried out in a furnace composed of three main zones; burning, annealing and bluing. The decarburizing atmosphere (CO/CO_2) was in the annealing zone, where in the bluing zone include applying bluing layer to insulate the decarburized annealed laminations.

The total time of the cycle was 10.4 hours, including 7.3 hrs. only in annealing stage to allow more time for grain growth process.

2.2 Material Characterizations

Tensile tests are run at a constant cross head speed of, 10 mm/min. Samples after hot rolling and primary recrystallization annealing and skin pass process were taken for tensile testing. Hardness measurements are taken for four points on the specimen surface utilizing TH320 Rockwell test, and the average value is then taken.

Determination of watt loss and magnetic permeability carried out according to standard EN 10126 at frequency of 50 HZ and at 1.5 Tesla, the measurements of magnetic polarization and specific total losses carried out using the 25cm Epstein frame device model IM 700-5, the test specimen was consisting of 32 Epstein strips. Half the test strips was cut parallel to the rolling direction and the other half in the perpendicular direction of rolling, giving an even distribution across the width of the material. The magnetic test was carried out only for temper rolled samples and for decarburized annealed samples as a final product.

Final decarburized samples were tested by estimating hysteresis curve using vibrating sample magnetometer device model 9600-1VSM, which usually used for measuring magnetic properties in materials [15], the device was operated at a constant frequency between a set of sense coils with magnetic moment resolution ± 0.02 full range and the hysteresis curves with magnetic properties was established for decarburized samples with 3,5 and 7% temper rolling reduction.

Standard processing techniques are used to examine the specimen's microstructure after various processing stages.

3. RESULTS AND DISCUSSION

3.1 Recrystallization mechanism

The optical microscopy of hot rolled specimen showed that the microstructure comprised of a lightly elongated ferrite grains with average grain size of $12.93\mu\text{m}$ as shown in Fig. (1).

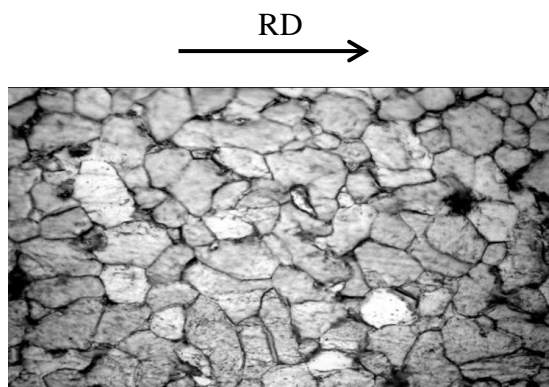


Figure 1. The optical micrograph of the as-received hot band at 500X

Following the various cold deformation of, 65, 70, 75% reduction, an increase of the hardness values of 81.5, 84, and 86 are obtained, this is mainly due to interaction with cold deformation. The microstructure observations for various cold reduction percentages indicated that heavily elongated grains are formed parallel to R.D and finer microstructure is observed with higher reduction.

Following the various cold reduction percentages, the steel is annealed at 740°C for 20 hrs., and the resulted microstructures are presented in Fig. 2 (A,B,C and D). It shows average grain sizes of 14. 15, 15.7 and 17µm obtained after 3, 5, 7 and 9% cold reduction respectively. These results indicated that grain refinement is involved in the recrystallization process. No visible grain growth is observed at this stage of annealing treatment.

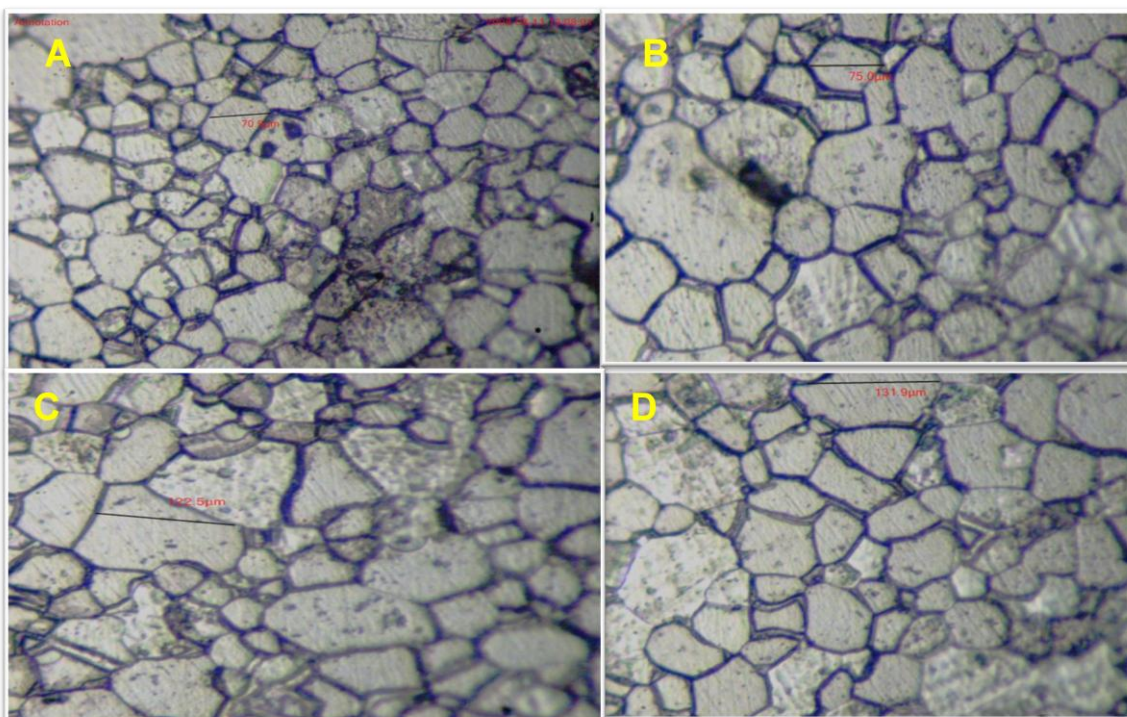


Figure 2. Microstructure of Samples after temper rolling: (A) 3, (B) 5, (C) 7 and (D) 9% reduction at 400X.

However, a heterogeneous grain size distribution is observed across the sheet thickness for all the various cold rolled samples. In some of the microstructure a wavy thick slip line appear inside the grain indicating that the structure is not fully recovered from the deformed state. Moreover, the rather thick grain boundaries observed in the microstructure suggest some kind of second phase precipitates are present, most likely to be of cementite types. Other types of precipitates is also possible to take place with the present steel either at grain boundary or inside the grains such as AlN, MnS and Fe₂O₃ precipitates. Recrystallization process is expected to start from the surface and progress toward the center. The onset of recrystallization at the surface is usually attributed to strain gradient developed during rolling process [16].

In the early stage of recrystallization annealing a temperature gradient exists across the steel cross section which will contribute to an early nucleation of the recrystallized grain compared to the sheet center. Therefore, the inhomogeneous grain size which is observed in the cross section of the sheet could also be attributed to such temperature distribution effects. Such a variation of grain size of the recrystallized structure could also be due to different grain stored. Recrystallized texture is determined by the texture nuclei formed at the early stage of the annealing treatment [1,4].

It is assumed that the nucleation step occurred in a region of high stored energy in two distinct ways: (i) The nucleation will form at low stored energy region that will grow on the expense of high stored energy area with the strain induced boundary mechanism (SIBM); (ii) On the other hand, it is possible that nucleation occurs through quick recovery of high stored energy and will grow into the unrecovered region [2, 17, 18].

In low carbon steel the stored deformation energy was assumed to be proportional to the slip system hardness and it observed to be lowest in a fibers orientations such as {100}<110> for the bcc structure ,while it is highest for γ fibers orientations such as {111}<110> and {111}<112> [10]. In the primary recrystallization there is mounting evidence that γ fibers orientations strengthen during the process on the expense of the non oriented grain rather than the fiber grain in the non-oriented silicon steel [17].

The tensile results after primary recrystallization stage are shown in Table: (2). The yield stress is dropped from 995 MPa after 75% cold deformation to 302MPa after recrystallization, due to recrystallization softing.

Table 2. Shows mechanical properties of as primary recrystallized annealed samples

Reduction Ratio%	Thickness Ma	Yield strength (MPa)	Tensile strength (Mpa)	EL%	HRS
65	0.7	320	401.0	29.4	47.8
70	0.6	232	425	30.35	46.6
75	0.5	302	417	32.14	44.3

The pre-strain of 75% reduction followed by primary recrystallized samples were temper rolled to various plastic strains of 3,5,7 and 9% at room temperature. This process is also, followed by the final decarburizing annealing treatment. The treatment is intended to stress relief the structure and promote grain growth to develop the optimum magnetic properties.

Only a slight increase in both yield and tensile stresses is obtained after temper rolling treatment. Optical micrograph for temper rolled specimen after 7and 9% temper rolling reductions are shown in Fig. (2). Moreover, the various stored energy during the temper rolling will be an additional energy for necessary grain boundaries movement during secondary recrystallization.

The decarburization annealing treatment microstructure of the various samples showed very clearly that grain growth took place, as shown in Fig. (3). Moreover, grain size measurement results as

function of temper rolling strain is presented in Table: (3) .From both annealing conditions A and B, a maximum of 85 and 91 μm grain sizes are obtained at the highest used strain of 9%. Grain growth is also evidence from hardness measurements which are observed to increase with temper rolling strain as shown in Table: (3). Microstructure after annealing process suggested that grain boundaries move along the decarburization front of the up normal grain growth and a relative wide grain size distribution are obtained. Furthermore, the grains are also observed to have a non-equiaxed shape and slightly elongated in the normal direction of the rolling plane.

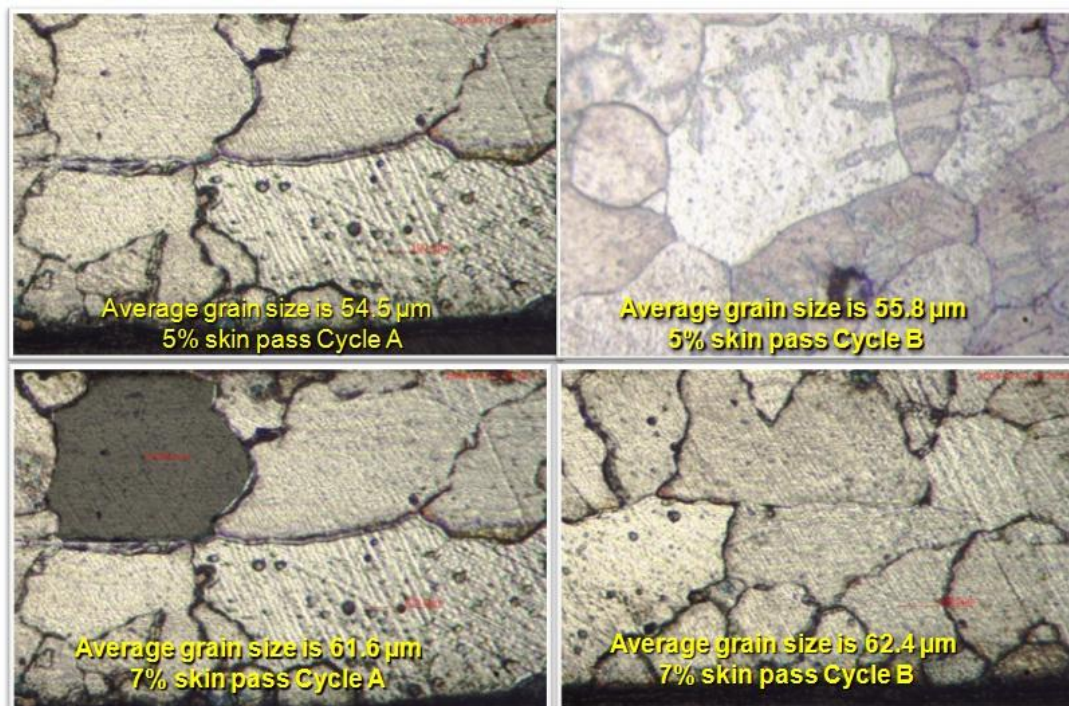


Figure 3. Shows the microstructure of decarburized annealed sample after 5% and 7% temper rolling for both cycle A and B. 400X

Table 3. Shows grain size and core losses and magnetic permeability related to different percent of temper rolling reduction and different decarburizing cycles.

Temper rolling conditions	Decarburized annealed results				
	Grain size μm		Watt loss W \ Kg at 1T		Magnetic Permeability B50 at 1T
Percent of reduction%	A	B	A	B	
0	32.2	34.2	3.443	3.231	6198
3	43.7	52.5	2.12	2.09	6328
5	52.5	55.8	0.0431	2.06	6876
7	60.6	62.4	2.0254	1.989	6945
9	85.4	92.1	2.051	2.032	6885

In a general term, the present results indicated that small prior plastic strain promote anomalous grain growth and this has been explained on the bases of strain induced grain boundary migration. In the annealing process and during heating stages for both used temperatures it is expected that at temperature below A_{c1} recrystallization occurs simultaneously with decarburization of the surface layer.

Once the temperature reach A_{c1} , the surface will be mainly of a ferrite structure, since phase transformation is not likely to occurs due to low carbon content after surface decarburization. However the inner region will transform to $(\alpha+\gamma)$ above A_{c1} . The nucleation will start from surface in the small regions of γ during its transformation to α -ferrite [17]. The temperature gradient also is likely to influence the secondary recrystallization process. It is to be noted that according to Fe- Si phase diagram, both recrystallization temperatures lies on the two phase zone $(\alpha +\gamma)$. The growth of grains will be diffusion controlled and the carbon diffusion along the grain boundaries produces an elastic stress causing motion of the latter [18]. For such mechanism the carbon concentration profile within the sheet cross section is not continuous, one due to difference in carbon solubility in ferrite and two phases zone $(\alpha +\gamma)$. At the end of decarburization process equilibrium concentration will be reached with a dominant ferrite grains structure all over the cross section.

Since the decarburization is proceeding in normal direction (ND) to the sheet plan toward the center, carbon in solid solution will preferentially enriched at the moving grain boundaries. Therefore, grain boundaries mobility will be reduced due to solute drag effects. Moreover, it has been argued that since the boundary velocity is proportional to the frequency of atoms jumping across the grain boundary plan while, decarburization accelerate atoms movement along the normal to sheet-plan [19]. Therefore, small pinning effect on the grain boundary that leads to directional boundary motion. Carbon content after decarburization annealing for both conditions A and B reached to 0.006 and 0.004 C% wt respectively compared with 0.053%C before annealing.

3.2 Magnetic properties

Magnetic properties are special qualities of electrical non-oriented steel compared to other materials. An optimum core loss is required and increase in magnetic flux to very high levels. Such properties are sensitive to process parameters mainly temper rolling and decarburization annealing condition. The observed increase in grain size with temper rolled strain percentage could be related to the decrease in watt loss measurement values as shown in Fig. (4) and, minimum is observed at grain size of- 62 μm ; However, with further coarsening in grains the trend is reverse to a higher watt- loss. It is therefore possible to consider that the optimum loss of pre strain is at 7% before decarburizing annealing. In general the effects of grain size can be divided in term of hysteresis and eddy current [20]. The present measurements for hysteresis curves as a function of pre-strain is shown in Table: (3). It is possible to conclude that a noticeable decrease of hysteresis loss is observed when grain size increase. This is related to the fact that grain boundary may hinder magnetic domain wall movements, and causes an increase of the loss. Table: (4) shows remnant magnetization as observed from hysteresis curves for decarburized annealed samples as function of the different temper rolling

reduction, the observed decrease in magnetization and hence the increase of magnetic permeability , the increase in grain size following the decarburization treatment. The optimum condition for highest permeability occurs at 7% pre-strain i.e., at 62μm grain size.

Table 4. Hysteresis curve for decarburized annealed samples of 3, 5 and 7% temper.

Percent of temper rolling %	Br (remanent magnetization emu/g)	Hc (coercive force Oe)
3	15.45	709.6
5	9.205	141.6
7	5.932	121.4

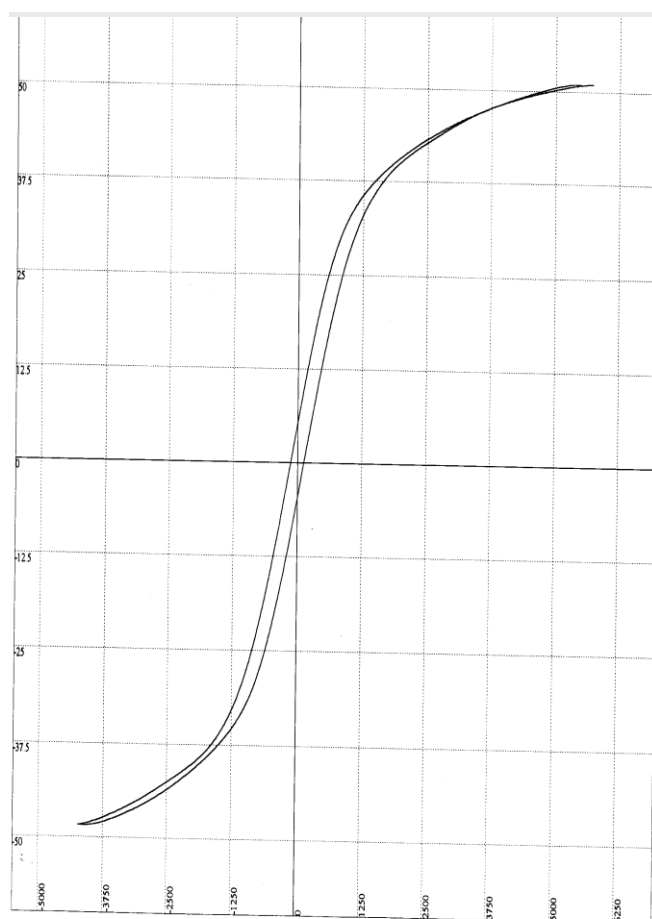


Figure 4. Hysteresis curve for decarburized annealed sample 5% temper rolled.

It is expected to decrease with increase grain size and hence increasing the magnetic permeability, this has been confirmed with the present results. The magnetic permeability measured at IT showed an increase of its values as grain size increases, Table: (3), while 9% per-strain with which

grain size reserve the trend. Therefore, the optimum conditions for highest permeability occur at 7% per strain i.e. at 62 μ m grain size.

4. CONCLUSION

In the present work, the effect of processing variables on magnetic properties of non-oriented electrical steel sheet is investigated. The starting material is hot rolled flat silicon steel sheet. The investigation presented results indicated that:

- Among the various cold reductions used in the present work, the 75% cold reduction is one which will has highest stored energy for the following primary recrystallization annealing carried out at 740°C.

- A grain refining is obtained as a function of pre-rolling reduction percentage with an average grain size of 14 μ m, with improved mechanical properties.

- Various temper rolling reductions are introduced before decarburization annealing process and the 7 to 9% temper reduction showed the best magnetic properties after the final stage of annealing.

- The final decarburization treatment resulted in a reduction in the carbon content from 0.054 to -0.004% C, and grain growth obtained is a function of temper rolling reduction. A maximum grain size of 92 μ m is obtained for 9% temper rolling.

ACKNOWLEDGEMENT

The authors extend their appreciation to the Deanship of Scientific Research at King Saud University for funding the work through the research group project No RGP-VPP-036.

References

1. Y. Kurosaki, H. Mogi, H. Fujii, T. Kubota, M. Shiozaki, *Journal of Magnetism and Magnetic Materials*, 320 (2008) 2474.
2. M. Yabumoto, C. Kaido, T. Wakisaka, T Kubota, N Suzuki, *Nippon Steel Tech. Rep.*, 88 (2003) 57.
3. O. Hubert, E. Hug, *Master Sci. Tech.*, 11 (1995) 482.
4. G. Loisos , A. J. Moses *Journal of Material Proc. Tech.*, 161 (2005) 15.
5. Y. Kurosaki, H. Mogi, H. Fujii, T. Kubota, M. Shiozaki, *Journal of Magnetism and Magnetic Materials*, 320 (2008) 2474
6. K. H. Schmidt, *Journal of Magnetism and Magnetic Materials*, 2 (1976) 136.
7. P. Baudouin, Y. Houbaert, S. Tumanski, *Journal of Magnetism and Magnetic Materials*, 254-255 (2003) 32.
8. L. Grigory, P.K. Rastogi, M. Bala, *Journal of Metals*, 38 (1986) 18.
9. J.T. Park, J.A. Szpunar, *Journal of Magnetism and Magnetic Materials*, 321 (2009) 1928.
10. J.T. Park, J.S. Woo, S.K. Chang, *Journal of Magnetism and Magnetic Materials*, 182 (1998) 381.
11. C.K. Hou, *Journal of Magnetism and Magnetic Materials*, 162 (1996) 291.
12. K. Matsumura, B. Fukuda , *IEEE Transactions on Magnetics*, 20 (1984) 1533.
13. A. Chaudhury, R. Khatirkar, N.N. Viswanathan, V. Singal, A. Ingle, S. Joshi, I. Samajdar, *Journal of Magnetism and Magnetic Materials*, 313 (2007) 21.

14. R. P. Kumar, I. Samajdar, N.N. Viswanathan, V. Singal, V. Seshadri, *Journal of Magnetism and Magnetic Materials*, 264 (2003) 75.
15. T. A. Salah El-Din, A. A. Elzatahry, D. M. Aldhayan, A. M. Al-Enizi, S.S. Al-Deyab, *Int. J. Electrochem. Sci.*, 6 (2011) 6177.
16. M. F. De Campos, M. J. Sablik, F. J. G. Landgraf, T. K. Hirsch, R. Machado, R. Magnabosco, C. J. Gutierrez, A. Bandyopadhyay, *Journal of Magnetism and Magnetic Materials*, 320 (2008) e377-e380.
17. J.T. Park, *Ph.D thesis*, Department of mining, material engineering McGill University Montreal, Canada,(2002).
18. L. Kestensi, S. Jacobs, *Texture, Stress, and Microstructure*, 2008 (2008) 1.
19. K. H. J. Buschow, F. R. de Boer, *Physics of Magnetism and Magnetic Materials*, KLUWER ACADEMIC PUBLISHERS; New York, 75 (2004).
20. A. Chaudhurya, R. Khatirkara, I, N.N. Viswanathana, V. Singalb, A. Ingleb, S. Joshib, I. Samajdara, *Journal of Magnetism and Magnetic Materials*, 313 (2007) 21.